

Dependencies of lepton angular distribution coefficients on the transverse momentum and rapidity of Z bosons produced in pp collisions at the LHC

Wen-Chen Chang,¹ Randall Evan McClellan,^{2,3} Jen-Chieh Peng,² and Oleg Teryaev⁴

¹*Institute of Physics, Academia Sinica, Taipei 11529, Taiwan*

²*Department of Physics, University of Illinois at Urbana-Champaign, Urbana, Illinois 61801, USA*

³*Thomas Jefferson National Accelerator Facility, Newport News, Virginia 23606, USA*

⁴*Bogoliubov Laboratory of Theoretical Physics, JINR, 141980 Dubna, Russia*

(Dated: September 22, 2017)

High precision data of lepton angular distributions for γ^*/Z production in pp collisions at the LHC, covering broad ranges of dilepton transverse momenta (q_T) and rapidity (y), were recently reported. Strong q_T dependencies were observed for several angular distribution coefficients, A_i , including $A_0 - A_4$. Significant y dependencies were also found for the coefficients A_1 , A_3 and A_4 , while A_0 and A_2 exhibit very weak rapidity dependence. Using an intuitive geometric picture, we show that the q_T and y dependencies of the angular distributions coefficients can be well described.

PACS numbers: 12.38.Lg, 14.20.Dh, 14.65.Bt, 13.60.Hb

I. INTRODUCTION

The angular distribution of leptons produced in the Drell-Yan process [1] remains a subject of considerable interest. The original Drell-Yan model offered a specific prediction of a transversely polarized virtual photon for collinear quark-antiquark annihilation, resulting in a $1 + \cos^2 \theta$ lepton angular distribution [1]. This prediction was in good agreement with the earliest data, which were dominantly from dileptons with low transverse momentum (q_T) [2, 3]. As the dilepton's transverse momentum becomes large, due to QCD effects involving emission of partons of large transverse momenta, the angular distribution would no longer be azimuthally symmetric. A general expression for the lepton angular distribution in the Drell-Yan process becomes [4]

$$\frac{d\sigma}{d\Omega} \propto 1 + \lambda \cos^2 \theta + \mu \sin 2\theta \cos \phi + \frac{\nu}{2} \sin^2 \theta \cos 2\phi, \quad (1)$$

where θ and ϕ refer to the polar and azimuthal angles of l^- (e^- or μ^-) in the rest frame of γ^* . The azimuthal dependencies of the lepton angular distributions are described by the parameters μ and ν . While $\lambda = 1$, $\mu = 0$, and $\nu = 0$ in the original Drell-Yan model [1], the presence of the intrinsic transverse momentum and QCD effects would allow $\lambda \neq 1$ and $\mu, \nu \neq 0$. However, it was predicted [4] that the deviation of λ from unity is precisely correlated with the coefficient of the $\cos 2\phi$ term, namely, $1 - \lambda = 2\nu$. This so-called Lam-Tung relation, expected to be insensitive to QCD corrections [5–8], was found to be significantly violated in pion-induced Drell-Yan experiments [9, 10]. The unexpectedly large violation of the Lam-Tung relation inspired many theoretical work [11–14], including the suggestion [14] that a nonperturbative effect originating from the novel transverse-momentum-dependent (TMD) Boer-Mulders function [15] can account for this violation. This suggestion was found to be consistent with the existing pion and proton induced Drell-Yan data [16]. It also led to first extractions of the Boer-Mulders functions from the

$\cos 2\phi$ dependence of the unpolarized Drell-Yan data [17, 18]. The azimuthal angular distributions of leptons in unpolarized or polarized Drell-Yan process are now regarded as an important tool for accessing the novel TMDs [14, 19–21].

At collider energies, measurement of lepton angular distributions in W and Z boson productions has long been advocated as a sensitive tool for understanding the production mechanism of these gauge bosons [22, 23]. The first measurement of the lepton angular distribution in γ^*/Z production was reported by the CDF Collaboration for $\bar{p}p$ collision at 1.96 TeV [24]. Very recently, the CMS [25] and ATLAS [26] Collaborations at the LHC reported high-statistics measurements of the lepton angular distribution of γ^*/Z production in pp collision at $\sqrt{s} = 8$ TeV. Strong q_T dependencies were observed for the λ , μ , and ν parameters. Moreover, violation of the Lam-Tung relation was found for these data at large q_T . Since the effects of TMD are expected to be negligible at large q_T , the presence of the Boer-Mulders function cannot explain the striking violation of the Lam-Tung relation at LHC energies.

In a recent paper [27], we showed that the observed q_T dependence of λ and ν , as well as the violation of the Lam-Tung relation, can be well described by a geometric picture. While it is important to compare perturbative QCD calculations with these data, it is also instructive to understand the essential features of these data in terms of an intuitive geometric picture. In this paper, we extend the previous work, which focuses on the λ and ν parameters and the Lam-Tung relation, to other angular distribution parameters. We also compare the striking q_T and rapidity (y) dependencies of the angular distribution coefficients measured at the LHC with our intuitive geometric picture. We find that many salient features of the data can be well understood within the framework of this simple and intuitive approach.

This paper is organized as follows. In Sec. II we present our model and derive some expressions relevant for understanding the lepton angular distributions for γ^*/Z production. We then compare calculations using this model with data on the q_T

and rapidity dependencies in Secs. III and IV, respectively. We conclude in Sec. V.

II. LEPTON ANGULAR DISTRIBUTION COEFFICIENTS

The lepton angular distribution in the γ^*/Z rest frame is expressed by both the CMS and ATLAS Collaborations as

$$\begin{aligned} \frac{d\sigma}{d\Omega} \propto & (1 + \cos^2 \theta) + \frac{A_0}{2}(1 - 3 \cos^2 \theta) + A_1 \sin 2\theta \cos \phi \\ & + \frac{A_2}{2} \sin^2 \theta \cos 2\phi + A_3 \sin \theta \cos \phi + A_4 \cos \theta \\ & + A_5 \sin^2 \theta \sin 2\phi + A_6 \sin 2\theta \sin \phi \\ & + A_7 \sin \theta \sin \phi, \end{aligned} \quad (2)$$

where θ and ϕ are the polar and azimuthal angles of l^- (e^- or μ^-) in the rest frame of γ^*/Z like in Eq. (1). Compared to Eq. (1), Eq. (2) contains several additional terms ($A_3 - A_7$), due to the presence of parity-violating coupling for the Z boson. It is clear that λ, μ, ν in Eq. (1) are related to A_0, A_1, A_2 via

$$\lambda = \frac{2 - 3A_0}{2 + A_0}; \quad \mu = \frac{2A_1}{2 + A_0}; \quad \nu = \frac{2A_2}{2 + A_0}. \quad (3)$$

Equation (3) shows that the Lam-Tung relation, $1 - \lambda = 2\nu$, becomes $A_0 = A_2$.

While Eq. (2) can be derived from the consideration of the general form of the lepton and hadron tensors involved in the γ^*/Z production, we present a derivation based on an intuitive geometric picture. We first define three different planes, i.e., the hadron plane, the quark plane, and the lepton plane, shown in Fig. 1. For nonzero q_T , the beam and target hadron momenta, \vec{P}_B and \vec{P}_T , are no longer collinear in the rest frame of γ^*/Z , and they form the ‘‘hadron plane’’ shown in Fig. 1. Various coordinate systems in the γ^*/Z rest frame have been considered in the literature, and the Collins-Soper (C-S) frame [28] was used by both the CMS and ATLAS Collaborations. For the Collins-Soper frame, the \hat{x} and \hat{z} axes both lie in the hadron plane, while the \hat{z} axis bisects \vec{P}_B and $-\vec{P}_T$ with an angle β . It is straightforward to show that

$$\tan \beta = q_T/Q, \quad (4)$$

where Q is the mass of the dilepton. Figure 1 also shows the ‘‘lepton plane’’ formed by the momentum vector of l^- and the \hat{z} axis. The l^- and l^+ are emitted back-to-back with equal momenta in the rest frame of γ^*/Z .

In the γ^*/Z rest frame, a pair of collinear q and \bar{q} with equal momenta annihilate into a γ^*/Z , as illustrated in Fig. 1. We define the momentum unit vector of q as \hat{z}' , and the ‘‘quark plane’’ is formed by the \hat{z}' and \hat{z} axes. The polar and azimuthal angles of the \hat{z}' axis in the Collins-Soper frame are denoted as θ_1 and ϕ_1 . The $q - \bar{q}$ axis, called the ‘‘natural’’ axis, has the important property [29] that the l^- angular distribution is azimuthally symmetric with respect to this axis, namely,

$$\frac{d\sigma}{d\Omega} \propto 1 + a \cos \theta_0 + \cos^2 \theta_0, \quad (5)$$

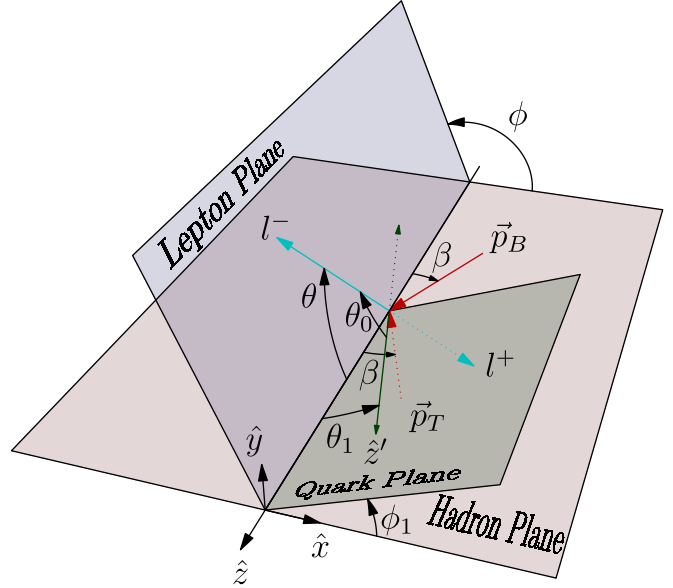


FIG. 1: Definition of the Collins-Soper frame and various angles and planes in the rest frame of γ^*/Z . The hadron plane is formed by \vec{P}_B and \vec{P}_T , the momentum vectors of the beam (B) and target (T) hadrons. The \hat{x} and \hat{z} axes of the Collins-Soper frame both lie in the hadron plane with the \hat{z} axis bisecting the \vec{P}_B and $-\vec{P}_T$ vectors. The quark (q) and antiquark (\bar{q}) annihilate collinearly with equal momenta to form γ^*/Z , while the quark momentum vector \hat{z}' and the \hat{z} axis form the quark plane. The polar and azimuthal angles of \hat{z}' in the Collins-Soper frame are θ_1 and ϕ_1 . The l^- and l^+ are emitted back-to-back with θ and ϕ as the polar and azimuthal angles for l^- .

where θ_0 is the angle between the l^- momentum vector and the \hat{z}' axis (see Fig. 1), and a is the forward-backward asymmetry originating from the parity-violating coupling to the Z boson. We recently showed [27] that Eq. (2) can be derived from Eq. (5) by noting that

$$\cos \theta_0 = \cos \theta \cos \theta_1 + \sin \theta \sin \theta_1 \cos(\phi - \phi_1). \quad (6)$$

Substituting Eq. (6) into Eq. (5), one obtains

$$\begin{aligned} \frac{d\sigma}{d\Omega} \propto & (1 + \cos^2 \theta) + \frac{\sin^2 \theta_1}{2}(1 - 3 \cos^2 \theta) \\ & + \left(\frac{1}{2} \sin 2\theta_1 \cos \phi_1\right) \sin 2\theta \cos \phi \\ & + \left(\frac{1}{2} \sin^2 \theta_1 \cos 2\phi_1\right) \sin^2 \theta \cos 2\phi \\ & + (a \sin \theta_1 \cos \phi_1) \sin \theta \cos \phi + (a \cos \theta_1) \cos \theta \\ & + \left(\frac{1}{2} \sin^2 \theta_1 \sin 2\phi_1\right) \sin^2 \theta \sin 2\phi \\ & + \left(\frac{1}{2} \sin 2\theta_1 \sin \phi_1\right) \sin 2\theta \sin \phi \\ & + (a \sin \theta_1 \sin \phi_1) \sin \theta \sin \phi. \end{aligned} \quad (7)$$

A comparison between Eq. (2) and Eq. (7) shows a one-to-one correspondence for all angular distribution terms. Moreover, the angular distribution coefficients $A_0 - A_7$ can now be ex-

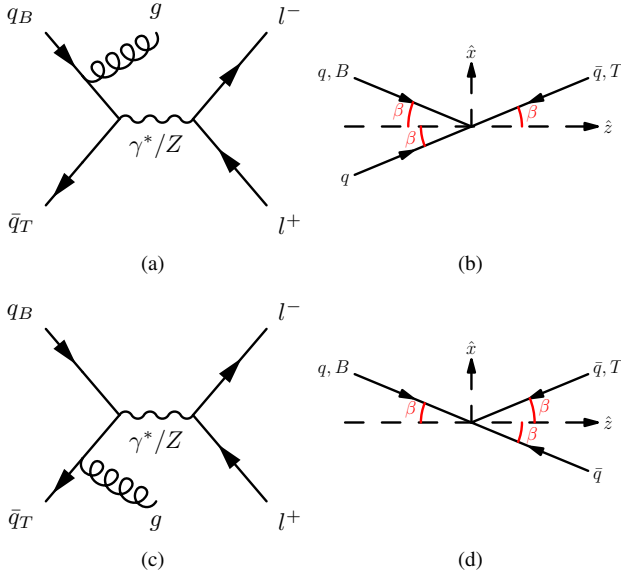


FIG. 2: (a) Feynman diagram for $q - \bar{q}$ annihilation where a gluon is emitted from a quark in the beam hadron (B). (b) Momentum direction for q and \bar{q} in the C-S frame before and after gluon emission. The momentum direction of q is now collinear with that of \bar{q} . (c) Feynman diagram for the case where a gluon is emitted from an antiquark in the target hadron (T). (d) Momentum direction for q and \bar{q} in the C-S frame before and after gluon emission for diagram (c).

pressed in terms of the quantities θ_1, ϕ_1 and a as follows:

$$\begin{aligned}
 A_0 &= \langle \sin^2 \theta_1 \rangle & A_1 &= \frac{1}{2} \langle \sin 2\theta_1 \cos \phi_1 \rangle \\
 A_2 &= \langle \sin^2 \theta_1 \cos 2\phi_1 \rangle & A_3 &= \langle a \sin \theta_1 \cos \phi_1 \rangle \\
 A_4 &= \langle a \cos \theta_1 \rangle & A_5 &= \frac{1}{2} \langle \sin^2 \theta_1 \sin 2\phi_1 \rangle \\
 A_6 &= \frac{1}{2} \langle \sin 2\theta_1 \sin \phi_1 \rangle & A_7 &= \langle a \sin \theta_1 \sin \phi_1 \rangle. \quad (8)
 \end{aligned}$$

The $\langle \cdot \cdot \cdot \rangle$ in Eq. (8) is a reminder that the measured values of A_i at given values of q_T and y are averaged over events having different values of θ_1, ϕ_1 and a , in general. Equation (8) is a generalization of an earlier work [30] which considered the special case of $\phi_1 = 0$ and $a = 0$.

The values of $A_0 - A_7$ are bounded by certain limits as a result of the properties of the trigonometric functions and $|a| < 1$. In particular, we obtain the following relations from Eq. (8):

$$\begin{aligned}
 0 &\leq A_0 \leq 1 & -1/2 &\leq A_1 \leq 1/2 \\
 -1 &\leq A_2 \leq 1 & -1 &\leq A_3 \leq 1 \\
 -1 &\leq A_4 \leq 1 & -1/2 &\leq A_5 \leq 1/2 \\
 -1/2 &\leq A_6 \leq 1/2 & -1 &\leq A_7 \leq 1. \quad (9)
 \end{aligned}$$

The bounds on A_0, A_1, A_2 , together with Eq. (3), imply that

$$-1/3 \leq \lambda \leq 1; \quad -1 \leq \mu \leq 1; \quad -1 \leq \nu \leq 1. \quad (10)$$

Some inequality relations among the various coefficients A_i can also be obtained from Eq. (8). In particular, A_0 and A_2

TABLE I: Angles θ_1 and ϕ_1 for four cases of gluon emission in the $q - \bar{q}$ annihilation process at order- α_s . The signs of A_0 to A_4 for the four cases are also listed.

Case	Gluon emitted from	θ_1	ϕ_1	A_0	A_1	A_2	A_3	A_4
1	Beam quark	β	0	+	+	+	+	+
2	Target antiquark	β	π	+	-	+	-	+
3	Beam antiquark	$\pi - \beta$	0	+	-	+	+	-
4	Target quark	$\pi - \beta$	π	+	+	+	-	-

satisfy the relation

$$A_0 \geq A_2. \quad (11)$$

Equation (8) shows that in the case of $\phi_1 = 0$ or π , i.e., the quark plane and hadron plane are coplanar, the Lam-Tung relation $A_0 = A_2$ is obtained. When Lam-Tung relation is violated, A_0 must be greater than A_2 or, equivalently, $1 - \lambda > 2\nu$.

While the values of θ_1, ϕ_1 , and A_i depend on the specific coordinate system chosen for the γ^*/Z rest frame, it is worth noting that the relations in Eqs. (8)-(11) are independent of this choice, as long as the \hat{x} and \hat{z} axes of the reference frame lie within the hadron plane. Examples of such reference frames include the Collins-Soper, Gottfried-Jackson, and the helicity frames. As a consequence, if the Lam-Tung relation is satisfied (or violated) in any of these frames, it will be satisfied (or violated) in all other frames.

As shown in Eq. (8), the q_T and y dependencies of the angular distribution coefficients, A_i , are entirely governed by the q_T and y dependencies of θ_1, ϕ_1 and a . We first consider the quantities θ_1 and ϕ_1 , ignoring the small intrinsic transverse momentum, k_T , of the partons. At the leading-order in α_s (α_s^0), the quark axis, \hat{z}' , is collinear with the \hat{z} axis. Hence, the result $\theta_1 = 0$ (or $\theta_1 = \pi$) is obtained, and Eq. (8) shows that all A_i except A_4 vanish.

At the next-to-leading order (NLO), α_s , a hard gluon or a quark (antiquark) is emitted so that γ^*/Z acquires nonzero q_T . Figure 2(a) shows a diagram for the $q - \bar{q}$ annihilation process in which a gluon is emitted from the quark in the beam hadron. In this case, the momentum vector of the quark is modified such that it becomes opposite to the antiquark's momentum vector in the rest frame of γ^*/Z . Since the antiquark's momentum direction is the same as the target hadron's momentum direction, the \hat{z}' axis is along the direction of $-\vec{p}_T$ (see Fig. 2(b)). From Fig. 1, it is evident that $\theta_1 = \beta$ and $\phi_1 = 0$ in this case. Similarly, for the case of Fig. 2(c), where a gluon is emitted from an antiquark in the target hadron, one obtains $\theta_1 = \beta$ and $\phi_1 = \pi$, as illustrated in Fig. 2(d). Analogous results with $\theta_1 = \pi - \beta$ and $\phi_1 = 0$ (or $\phi = \pi$) can be found when the roles of beam and target are interchanged, as illustrated in Fig. 3. Table I lists the values of θ_1 and ϕ_1 for the four cases considered above. Given $\theta_1 = \beta$ (or $\theta_1 = \pi - \beta$) and $\tan \beta = q_T/Q$ in the Collins-Soper frame, we obtain the following results, relevant for the coefficients A_i in Eq. (8),

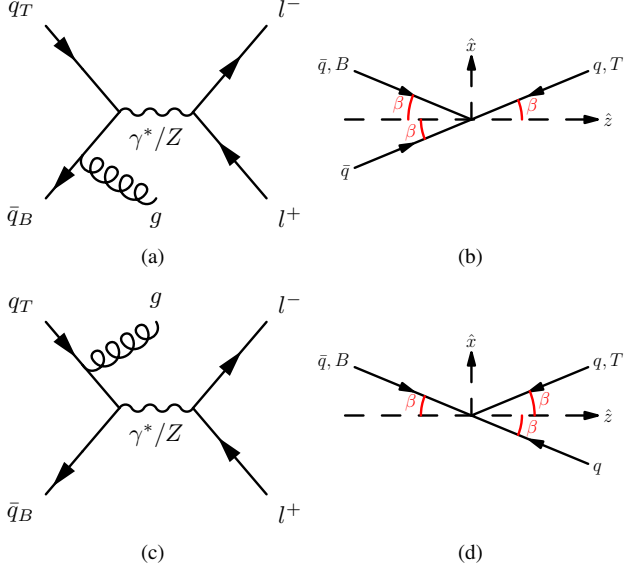


FIG. 3: (a) Feynman diagram for $q - \bar{q}$ annihilation where a gluon is emitted from an antiquark in the beam hadron (B). (b) Momentum direction for q and \bar{q} in the C-S frame before and after gluon emission. The momentum direction of q is now collinear with that of \bar{q} . (c) Feynman diagram for the case where a gluon is emitted from a quark in the target hadron (T). (d) Momentum direction for q and \bar{q} in the C-S frame before and after gluon emission for diagram (c).

for the NLO $q - \bar{q}$ annihilation processes:

$$\begin{aligned}
 \sin \theta_1 &= q_T / (Q^2 + q_T^2)^{1/2} \\
 \cos \theta_1 &= \pm Q / (Q^2 + q_T^2)^{1/2} \\
 \sin^2 \theta_1 &= q_T^2 / (Q^2 + q_T^2) \\
 \sin 2\theta_1 &= \pm 2q_T Q / (Q^2 + q_T^2), \quad (12)
 \end{aligned}$$

where the + (-) sign corresponds to $\theta_1 = \beta$ ($\theta_1 = \pi - \beta$). Since $\phi_1 = 0$ or π , one can see from Table I and Eq. (8) that the Lam-Tung relation, $A_0 = A_2$, is satisfied. Moreover, $A_5 - A_7$ must vanish, since they are proportional to $\sin \phi_1$ or $\sin 2\phi_1$, which are identically zero.

We next consider the Compton process at NLO. Unlike the cases for the $q - \bar{q}$ initial state shown in Figs. 2 and 3 where a hard gluon is emitted, a hard quark or antiquark will now accompany the γ^*/Z final state. Fig. 4(a) shows the diagram in which a gluon from the target hadron splits into a $q - \bar{q}$ pair and the quark from the beam hadron annihilates with the antiquark into a γ^*/Z . Since the momentum vector of the quark in the beam hadron is unchanged, $\theta_1 = \beta$ and $\phi_1 = \pi$, as shown in Fig. 4(b). This result is identical to that for the $q\bar{q}$ initial state shown in Fig. 2(d). Analogous results are obtained when gluon is emitted from the beam hadron, or when an antiquark replaces the quark in the initial state. However, a different situation is shown in Fig. 4(c), where the quark and gluon fuse into a quark, which then emits a γ^*/Z . As indicated in Fig. 4(d), θ_1 must satisfy $\beta \leq \theta_1 \leq \pi - \beta$, since the momenta of the initial quark and gluon combine vectorially, resulting in

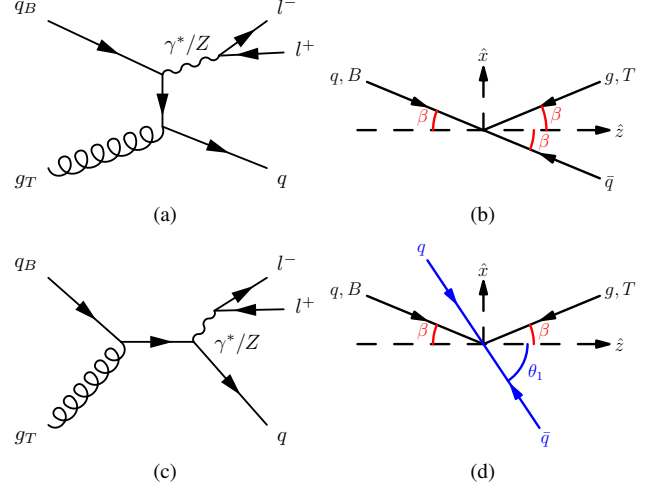


FIG. 4: (a) Feynman diagram for qG Compton process where a quark from the beam hadron annihilates with an antiquark from the splitting of a gluon in the target hadron. (b) Momentum direction of q , \bar{q} and gluon in the C-S frame before and after gluon splitting. (c) Feynman diagram for qG fusing into a quark which then emits a γ^*/Z . (d) Momentum direction of q , \bar{q} and gluon before and after the qG fusion.

a θ_1 within these limits. Therefore, the two distinct Compton processes would lead to a mean θ_1 larger than β , with the exact value governed by the relative weight of these two processes. It was shown by Thews [31] that, to a very good approximation, A_0 satisfies the relation, $A_0 = 5q_T^2 / (Q^2 + 5q_T^2)$. Since $A_0 = \sin^2 \theta_1$, we obtain, for the qG Compton processes at order α_s , the following expressions

$$\begin{aligned}
 \sin \theta_1 &= \sqrt{5}q_T / (Q^2 + 5q_T^2)^{1/2} \\
 \cos \theta_1 &= \pm Q / (Q^2 + 5q_T^2)^{1/2} \\
 \sin^2 \theta_1 &= 5q_T^2 / (Q^2 + 5q_T^2) \\
 \sin 2\theta_1 &= \pm 2\sqrt{5}q_T Q / (Q^2 + 5q_T^2). \quad (13)
 \end{aligned}$$

The + and - sign corresponds to $\theta_1 \leq \pi/2$ and $\theta_1 \geq \pi/2$, respectively.

We now consider the parity-violating forward-backward asymmetry, a , in Eqs. (5) and (8). The electroweak theory for Z boson production gives $a = 2A_f A_{f'}$ for the $f + \bar{f} \rightarrow Z \rightarrow f' + \bar{f}'$ process, where A_f is given as

$$A_f = \frac{2C_V^f C_A^f}{(C_V^f)^2 + (C_A^f)^2}. \quad (14)$$

The vector C_V^f and axial vector C_A^f couplings for Z boson to fermion f are, respectively, $I_W^3 - 2Q \sin^2 \theta_W$ and I_W^3 , where I_W^3 and θ_W denote the weak-isospin third component and the Weinberg angle. Using $\sin^2 \theta_W = 0.2315$, then Eq. (14) gives $a = 0.211$ for $u\bar{u} \rightarrow Z \rightarrow l^- l^+$, and $a = 0.299$ for $d\bar{d} \rightarrow Z \rightarrow l^- l^+$, where l refers to e or μ . We note that a has a positive value. Moreover, depending on the relative weight between the $u\bar{u}$ and the $d\bar{d}$ contributions, one expects the mean value of a to vary between these two limits.

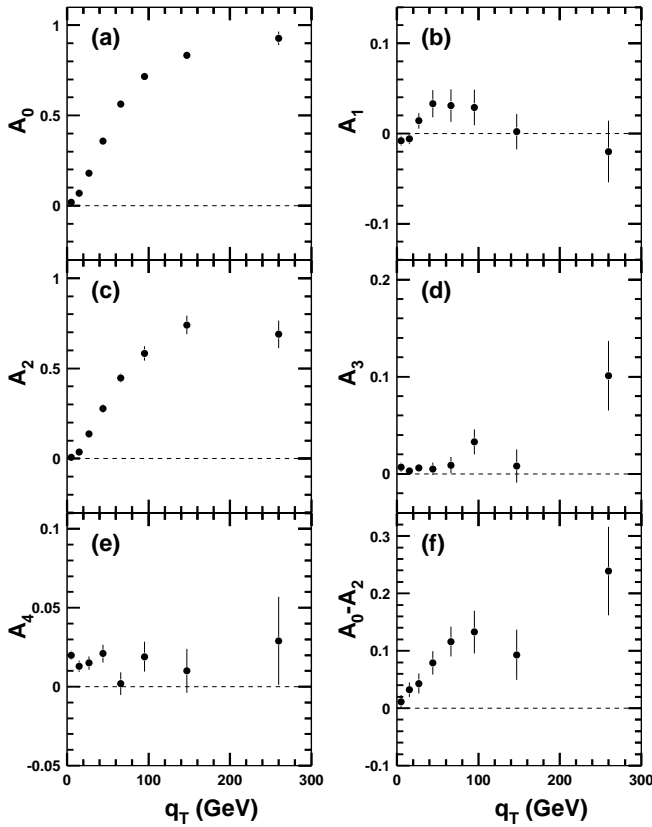


FIG. 5: The CMS data [25] on angular distribution coefficients A_i versus q_T for $|y| < 1.0$.

III. TRANSVERSE MOMENTUM DEPENDENCIES OF ANGULAR DISTRIBUTION COEFFICIENTS

We now compare the γ^*/Z production data at the LHC with calculations based on the results obtained in Sec. II. The LHC data cover a broad range in the dilepton's q_T and rapidity y ($0 < q_T < 600$ GeV and $0 < |y| < 3.5$). For simplicity, we only consider the CMS data in this work. The ATLAS data contain both the $\mu^-\mu^+$ and e^-e^+ dilepton events, doubling the statistics compared to the $\mu^-\mu^+$ data sample in CMS. However, the procedure of “regularization” adopted by the ATLAS Collaboration introduces model dependencies associated with the theoretical calculations used in the procedure. Although the tabulated uncertainties of the ATLAS data [26] are significantly smaller than that of the CMS data [25], it is difficult to assess the systematic uncertainties associated with the procedure of “regularization”. We therefore prefer to compare our calculations with the results of CMS, where a conventional analysis procedure without “regularization” is adopted.

Figure 5 shows the angular distribution coefficients A_i at the mid-rapidity region $|y| < 1.0$ measured by the CMS Collaboration. Some salient features in the q_T dependencies of A_i are observed. Figure 5 shows that the coefficients $A_0 - A_3$ are

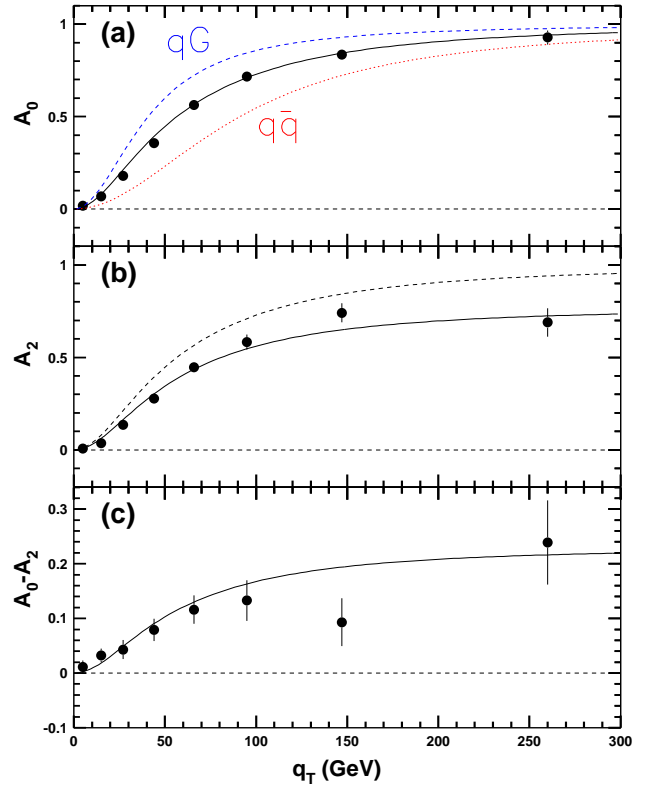


FIG. 6: Comparison between the CMS data [25] on A_0 , A_2 and $A_0 - A_2$ with calculations. Curves correspond to calculations described in the text.

consistent with zero at the smallest value of q_T . On the other hand, the coefficient A_4 is nonzero at $q_T \rightarrow 0$. The values of $A_5 - A_7$ are found by the CMS Collaboration to be consistent with zero [25]. In order to understand these general features of the angular distribution coefficients, Eq. (8) suggests that one could examine the properties of the quantities θ_1 and ϕ_1 .

From Eqs. (8), (12), (13), noting that $\phi_1 = 0$ or π and the γ^*/Z cross sections are dominated by the NLO $q\bar{q}$ and qG processes depicted in Figs. 4 and 5, one can readily predict the following patterns for the q_T dependencies of A_0 up to A_4 :

1) As $q_T \rightarrow 0$, Eqs. (8), (12), (13) show that A_0, A_1, A_2, A_3 all approach zero, since $\theta_1 \rightarrow 0$. On the other hand, A_4 is at its maximal value, since it is proportional to $\cos \theta_1$. As $q_T \rightarrow \infty$, θ_1 approaches the value of $\pi/2$, and A_0, A_2, A_3 reach their maximal values, while A_1 and A_4 approach zero. As shown in Fig. 5, the data are consistent with these expectations.

2) According to Eqs. (8), (12), (13) the values of A_0 would go from zero at $q_T = 0$ to unity as $q_T \rightarrow \infty$. At all values of q_T , one expects $A_2 \leq A_0$. In the case of $\cos 2\phi_1 = 1$, which occurs for the NLO processes as discussed above, the Lam-Tung relation, $A_0 = A_2$ is satisfied. When the Lam-Tung relation is violated, $A_0 \neq A_2$ (or $1 - \lambda \neq 2\nu$), it is expected that only $A_0 - A_2 > 0$ (or $1 - \lambda - 2\nu > 0$), not the alternative inequality $A_0 - A_2 < 0$, can occur. These expectations are

consistent with the data shown in Fig. 5.

3) As A_1 is proportional to $\sin 2\theta_1$, it would first increase with q_T , reaching a maximum, and then decrease. This is in contrast to A_0, A_2 , and A_4 , which are expected to increase with q_T monotonically. Similarly, A_4 would decrease monotonically with q_T , as it is proportional to $\cos \theta_1$. The data are consistent with these expected trends.

4) The upper and lower bounds on A_i , listed in Eq. (9), are well satisfied by the data.

We next compare the CMS data on the angular distribution coefficients A_0 to A_4 with calculations based on the intuitive geometric picture discussed above.

Figure 6(a) shows the values of A_0 versus q_T for $|y| < 1.0$. The dotted and dashed curves correspond to calculations using Eq. (8) and Eqs. (12), (13) for the $q\bar{q}$ and qG processes, $A_0 = q_T^2/(Q^2 + q_T^2)$ and $A_0 = 5q_T^2/(Q^2 + 5q_T^2)$, respectively. Note that the $q\bar{q}$ process alone underestimates A_0 , while the qG process overestimates it. Since these two processes contribute incoherently to the γ^*/Z production due to their distinct initial and final states (see Figs. 2-4), the observed A_0 is the result of an incoherent sum of these two processes. A best fit to the data, shown as the solid curve in Fig. 6(a), is obtained with a mixture of $58.5 \pm 1.6\%$ qG and $41.5 \pm 1.6\%$ $q\bar{q}$ processes. The excellent agreement between the data and the calculation lends support to the adequacy of this intuitive geometric picture. It also suggests that higher-order QCD processes do not affect the values of θ_1 (and A_0) significantly.

Figure 6(b) displays A_2 versus q_T for the $|y| < 1.0$ data from CMS. Eq. (8) shows that the value of A_2 should be identical to that of A_0 if $\phi_1 = 0$ or π . The dashed curve in Fig. 6(b) is identical to the solid curve in Fig. 6(a), obtained with a mixture of 58.5% qG and 41.5% $q\bar{q}$ processes. The deviation of the dashed curve from the data shows that the Lam-Tung relation, $A_0 = A_2$, is violated. From Eq. (8), it is evident that this violation is due to $\phi_1 \neq 0$ or π , namely, the quark and hadron planes are not coplanar. This noncoplanarity is caused by higher-order processes, in which multiple partons accompany the γ^*/Z in the final state. The hadron plane then contains the vector sum of multiple partons, and is in general not coplanar with respect to the quark plane. The effect of the noncoplanarity is to reduce the value of A_2 with respect to that of A_0 . The solid curve in Fig. 6(b), obtained with an overall reduction factor of 0.77, describes the CMS A_2 data well. This reduction factor, originating from the $\cos 2\phi_1$ factor, indicates that the effective value of the noncoplanarity angle, ϕ_1 , is around 20° . Figure 6(c) shows the q_T dependence of $A_0 - A_2$ for $|y| < 1.0$. The violation of the Lam-Tung relation, reflected by the nonzero values of $A_0 - A_2$, is well described by the solid curve taking into account the overall reduction factor of 0.77 for A_2 .

We next consider the coefficient A_1 . From Eq. (3), the coefficient A_1 is related to the parameter μ measured in fixed-target Drell-Yan experiments. In pp collision, A_1 is odd under $y \leftrightarrow -y$ exchange. Figure 7(a) shows the q_T dependence of A_1 measured at CMS. The sign of A_1 measured at negative y is flipped before combining it with A_1 measured at positive

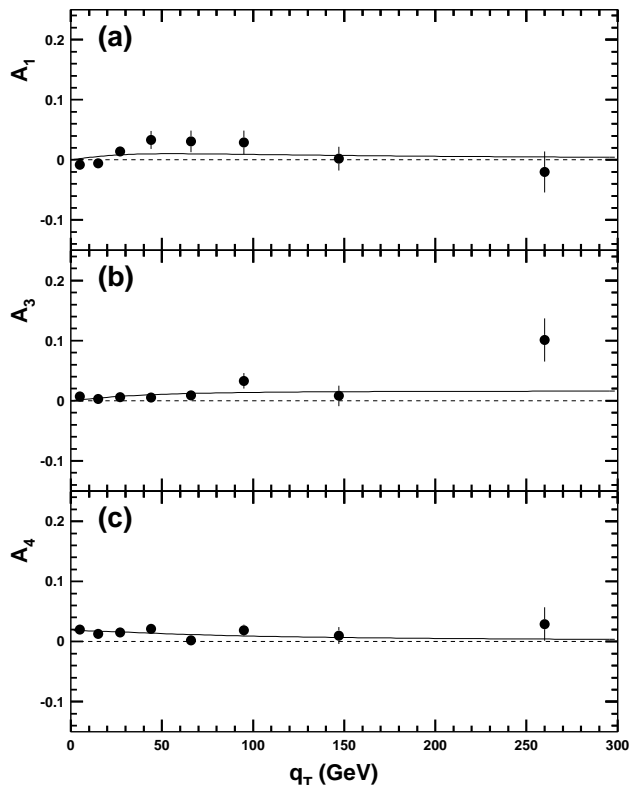


FIG. 7: Comparison between the CMS data [25] on A_1, A_3 and A_4 at $|y| < 1.0$ with calculations. Curves correspond to calculations described in the text.

y . Equation (8) shows that A_1 is given as $1/2 \langle \sin 2\theta_1 \cos \phi_1 \rangle$. The values of $\sin 2\theta_1$ are given in Eqs. (12) and (13) for the $q\bar{q}$ and qG processes, and $\phi_1 = 0$ (or π). For various cases as listed in Table I, one can calculate the values of A_1 for the four cases. Depending on the value of ϕ_1 , the sign of A_1 can be positive or negative, as shown in Table I. Hence, one expects a significant cancellation among contributions from processes with $\phi_1 = 0$ or $\phi_1 = \pi$. The solid curve in Fig. 7(a) is obtained with the following expression

$$A_1 = r_1 \left[f \frac{q_T Q}{Q^2 + q_T^2} + (1 - f) \frac{\sqrt{5} q_T Q}{Q^2 + 5q_T^2} \right], \quad (15)$$

where f is the fraction of $q\bar{q}$ process, $f = 0.415$, deduced from the A_0 data discussed earlier. The $\sin 2\theta_1$ values for the $q\bar{q}$ and qG processes given in Eqs. (12) and (13) are weighted by f and $1 - f$, respectively. The reduction factor r_1 represents the combined effect of the partial cancellation discussed above and the deviation of ϕ_1 from 0 or π due to higher-order QCD. The best-fit value of r_1 using Eq. (15) is $r_1 = 0.0215$. The small value of r_1 indicates the presence of a strong cancellation at small values of y .

Similar considerations also apply to the coefficient A_3 , which is also an odd function of y in pp collision. Both A_1 and A_3 are sensitive to $\cos \phi_1$. Table I shows the signs of A_3 for four different cases in $q\bar{q}$ process. As a parity-violating ob-

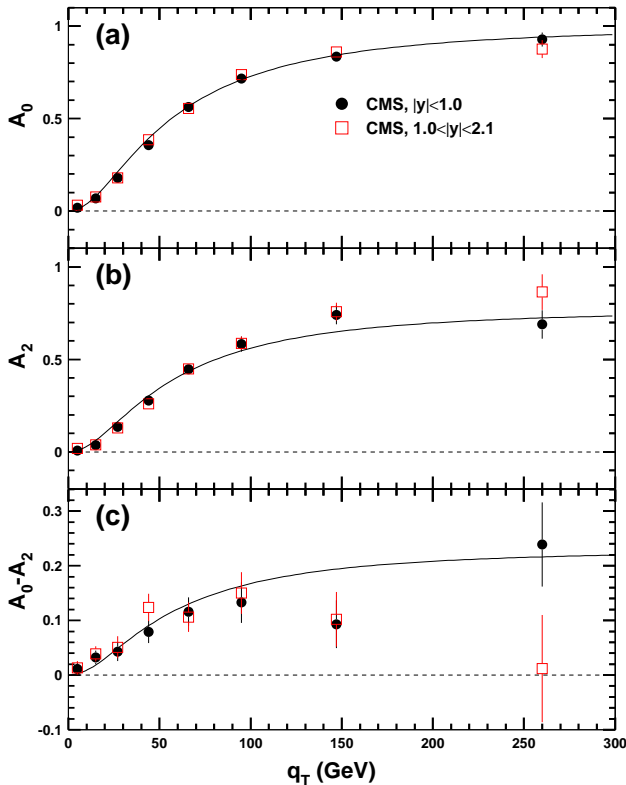


FIG. 8: Comparison between the CMS data [25] on A_0 and A_2 at two rapidity regions with calculations. Curves correspond to calculations described in the text.

servable, A_3 is also sensitive to the forward-backward asymmetry parameter a . The solid curve in Fig. 7(b) corresponds to the following expression

$$A_3 = r_3 \left[f \frac{q_T}{(Q^2 + q_T^2)^{1/2}} + (1-f) \frac{\sqrt{5}q_T}{(Q^2 + 5q_T^2)^{1/2}} \right]. \quad (16)$$

Equation (16) is analogous to Eq. (15), except that the reduction factor r_3 now includes an additional contribution from a . The best-fit value, $r_3 = 0.0163$, is obtained. As shown in Fig. 7(b), the agreement between the data and this simple calculation is reasonable.

Figure 7(c) shows A_4 versus q_T for $|y| < 1.0$. Unlike all other coefficients, A_4 has a nonzero value as q_T approaches zero. As discussed earlier, this is well explained by its dependence on $\cos \theta_1$, which has a maximal value at $q_T = 0$. The solid curve in Fig. 7(c) is obtained with the following expression

$$A_4 = r_4 \left[f \frac{Q}{(Q^2 + q_T^2)^{1/2}} + (1-f) \frac{Q}{(Q^2 + 5q_T^2)^{1/2}} \right], \quad (17)$$

where the best-fit value for the reduction factor r_4 is 0.0183. Both r_3 and r_4 contain the parity violating parameter a . However, unlike r_3 , r_4 does not contain the $\cos \phi_1$ term. This qualitatively explains the slightly larger value for r_4 than r_3 . The

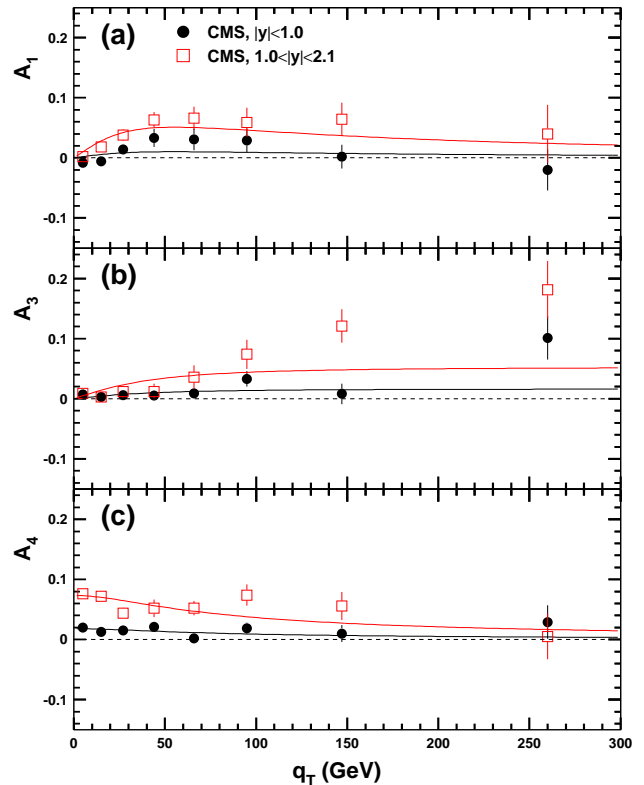


FIG. 9: Comparison between the CMS data [25] on A_1 , A_3 and A_4 at two rapidity regions with calculations. Curves correspond to calculations described in the text.

calculation based on Eq. (17) is in very good agreement with the data shown in Fig. 7(c).

IV. RAPIDITY DEPENDENCIES OF ANGULAR DISTRIBUTION COEFFICIENTS

The CMS Collaboration has reported the rapidity dependencies of A_i for two bins, $|y| < 1.0$ and $1.0 < |y| < 2.1$. In this Section, we compare the measured y dependencies with expectations based on our intuitive geometric picture. Figure 8 shows that for A_0 and A_2 , there are very weak, if any, rapidity dependencies. The solid curves in Fig. 8 are taken from the calculations shown in Fig. 6. It is evident that data at both rapidity bins are well described by a single curve. The weak rapidity dependence of A_0 reflects the fact that A_0 only depends on θ_1 , which, according to Eqs. (12) and (13), is independent of the rapidity y . However, higher-order QCD effects can introduce weak rapidity dependence for A_0 . The weak rapidity dependence for A_2 shows that ϕ_1 is weakly y dependent. Indeed, at order α_s , Table I shows that $\cos 2\phi_1$ is equal to unity for all four cases, independent of the value of y . Again, higher-order QCD will allow $\cos 2\phi_1$ to deviate from unity, but the deviation has a very weak y dependence.

In striking contrast to A_0 and A_2 , the coefficients A_1, A_3

TABLE II: Reduction factors r_i for A_1, A_3, A_4 for two rapidity bins.

	$ y < 1.0$	$1.0 < y < 2.1$
r_1	0.0215	0.11
r_3	0.0113	0.0524
r_4	0.0181	0.0732

and A_4 exhibit pronounced rapidity dependencies, as shown in Fig. 9. A common feature for A_1, A_3 and A_4 is that they all rise significantly as y increases. An intuitive explanation for this strong y dependence is as follows. Table I shows that the various contributions to A_1, A_3 and A_4 can be positive or negative, and each contribution is weighted by the corresponding density distributions for the interacting partons. At small values of y , the momentum fraction carried by the beam parton, (x_B), is comparable to that of the target parton, (x_T). Hence the weighting factors for various cases are of similar magnitude and the net contribution is small due to partial cancellations among them. On the other hand, as y becomes large, x_B becomes significantly larger than x_T . Hence, the weighting factors are now dominated by fewer terms, resulting in less cancellation and a larger net result. The various curves shown in Fig. 9 correspond to calculations using Eqs. (15), (16), (17), respectively, for A_1, A_3 and A_4 . The CMS data are quite well described by the best-fit values of r_1, r_3 , and r_4 listed in Table II.

V. SUMMARY AND CONCLUSIONS

We have presented an intuitive interpretation for the lepton angular distribution coefficients for γ^*/Z production measured at the LHC. We first derive the general expression [Eq. (7)] for the lepton polar and azimuthal angular distributions in the dilepton rest frame, starting from the azimuthally symmetric lepton angular distribution [Eq. (5)] with respect to the quark-antiquark axis. We show that the various angular distribution coefficients are governed by three quantities, θ_1, ϕ_1 and a (Eq. 8). The upper and lower bounds [Eq. (9)] for the angular distribution coefficients are obtained as a result of the expressions in Eq. (8). Similarly, the inequality relation between A_0 and A_2 , relevant for the violation of the Lam-Tung relation, is obtained [Eq. (11)].

We then consider the characteristics of the quantities θ_1, ϕ_1 and a . The expressions for θ_1 and ϕ_1 are obtained for both the $q\bar{q}$ and qG processes at order α_s . The q_T dependence of A_0 is found to be very well described using the results for θ_1 . It also allows a determination of the relative fractions of these two processes. This result is noteworthy, since it shows that a measurement of the angular distribution coefficient A_0 alone could lead to important information on the dynamics of the production mechanism, namely, the relative contribution of the $q\bar{q}$ annihilation and the qG Compton processes.

The CMS data clearly show that the Lam-Tung relation, $A_0 = A_2$, is violated. The origin of this violation is attributed in our approach to the deviation of $\cos 2\phi_1$ from unity, indicating the noncoplanarity between the hadron and quark planes. This noncoplanarity is caused by higher-order QCD processes. We show that the amount of noncoplanarity can be deduced from the $A_0 - A_2$ data directly. We have also compared our approach with the CMS data for other angular distribution coefficients, A_1, A_3, A_4 , and found that their q_T dependencies, governed by the q_T dependence of θ_1 , can be well described.

We also show that the rapidity dependencies of the A_i can be well understood in this intuitive approach. In particular, the weak rapidity dependencies of the A_0 and A_2 , and the pronounced rapidity dependencies for A_1, A_3 and A_4 can be explained by the absence or presence of cancellation effects, which depend strongly on the rapidity.

We note that the intuitive approach presented in this paper is by no means a substitute for the perturbative QCD calculations. The goal of this work is to provide some intuitive explanation of some salient features present in the lepton angular distribution data. This could offer some useful insights on the origins of many interesting characteristics of the lepton angular distributions which are being measured at the LHC with high precision.

The present approach could also be extended to fixed-target Drell-Yan experiments. Some recent work [32] shows the importance of the perturbative QCD effects even at fixed-target energies. A comparison between this intuitive approach and the perturbative QCD calculations is also of interest. It is also promising to extend this intuitive approach to some other processes with hadron or lepton beams.

ACKNOWLEDGEMENT

This work was supported in part by the U.S. National Science Foundation and the Ministry of Science and Technology of Taiwan.

-
- [1] S.D. Drell and T.M. Yan, Phys. Rev. Lett. **25**, 316 (1970); Ann. Phys. (NY) **66**, 578 (1971).
 - [2] I. R. Kenyon, Rep. Prog. Phys. **45**, 1261 (1982).
 - [3] P.L. McGaughey, J.M. Moss, and J.C. Peng, Annu. Rev. Nucl. Part. Sci. **49**, 217 (1999).
 - [4] C.S. Lam and W.K. Tung, Phys. Rev. D **18**, 2447 (1978).
 - [5] J.C. Collins, Phys. Rev. Lett. **42**, 291 (1979).
 - [6] C.S. Lam and W.K. Tung, Phys. Rev. D **21**, 2712 (1980).
 - [7] D. Boer and W. Vogelsang, Phys. Rev. D **74**, 014004 (2006).
 - [8] E.L. Berger, J.W. Qiu, and R.A. Rodriguez-Pedraza, Phys. Lett. B **656**, 74 (2007).
 - [9] NA10 Collaboration, S. Falciano *et al.*, Z. Phys. C **31**, 513 (1986); M. Guanziroli *et al.*, Z. Phys. C **37**, 545 (1988).
 - [10] E615 Collaboration, J.S. Conway *et al.*, Phys. Rev. D **39**, 92 (1989); J.G. Heinrich *et al.*, Phys. Rev. D **44**, 1909 (1991).

- [11] A. Brandenburg, S.J. Brodsky, V.V. Khoze, and D. Müller, Phys. Rev. Lett. **73**, 939 (1994).
- [12] K.J. Eskola, P. Hoyer, M. Vätinnen, and R. Vogt, Phys. Lett. B **333**, 526 (1994).
- [13] A. Brandenburg, O. Nachtmann, and E. Mirkes, Z. Phys. C **60**, 697 (1993).
- [14] D. Boer, Phys. Rev. D **60**, 014012 (1999).
- [15] D. Boer and P.J. Mulders, Phys. Rev. D **57**, 5780 (1998).
- [16] Fermilab E866 Collaboration, L.Y. Zhu *et al.*, Phys. Rev. Lett. **99**, 082301 (2007); Phys. Rev. Lett. **102**, 182001 (2009).
- [17] B. Zhang, Z. Lu, B.-Q. Ma, and I. Schmidt, Phys. Rev. D **77**, 054011 (2008).
- [18] V. Barone, S. Melis, and A. Prokudin, Phys. Rev. D **82**, 114025 (2010).
- [19] S. Arnold, A. Metz, and M. Schlegel, Phys. Rev. D **79**, 034005 (2009).
- [20] J. Huang, Z.B. Kang, I. Vitev, and H. Xing, Phys. Rev. D **93**, 014036 (2016).
- [21] J.C. Peng and J.W. Qiu, Prog. Part. Nucl. Phys. **76**, 43 (2014).
- [22] E. Mirkes and J. Ohnemus, Phys. Rev. D **50**, 5692 (1994).
- [23] E.L. Berger, L.E. Gordon, and M. Klasen, Phys. Rev. D **58**, 074012 (1998).
- [24] CDF Collaboration, T. Aaltonen *et al.*, Phys. Rev. Lett. **106**, 241801 (2015).
- [25] CMS Collaboration, V. Khachatryan *et al.*, Phys. Lett. B **750**, 154 (2011).
- [26] ATLAS Collaboration, G. Aad *et al.*, J. High Energy Phys. **08** 159 (2016).
- [27] J.C. Peng, W.C. Chang, R.E. McClellan, and O. Teryaev, Phys. Lett. B **758**, 384 (2016).
- [28] J.C. Collins and D.E. Soper, Phys. Rev. D **16**, 2219 (1977).
- [29] P. Faccioli, C. Lourenco, J. Seixas, and H. Wohri, Phys. Rev. D **83**, 056008 (2011).
- [30] O.V. Teryaev, Proceedings of XI Advanced Research Workshop on High Energy Spin Physics, Dubna, 2005, p. 171.
- [31] R.L. Thews, Phys. Rev. Lett. **43**, 987 (1979).
- [32] M. Lambertsen and W. Vogelsang, Phys. Rev. D **93**, 114013 (2016).